

# XMM-Newton observation of the ultraluminous quasar SDSS J010013.02+280225.8 at redshift 6.326

Yanli Ai<sup>1</sup>★, A.C. Fabian<sup>2</sup>, Xiaohui Fan<sup>3</sup>, S.A. Walker<sup>2,4</sup>, G. Ghisellini<sup>5</sup>, T. Sbarrato<sup>6</sup>,  
Liming Dou<sup>7</sup>, Feige Wang<sup>8</sup>, Xue-Bing Wu<sup>9,8</sup>, Longlong Feng<sup>1</sup>

<sup>1</sup>*School of Physics and Astronomy, Sun Yat-Sen University, Guangzhou 510275, China, aiyanli@mail.sysu.edu.cn*

<sup>2</sup>*Institute of Astronomy, Madingley Road, Cambridge CB3 0HA, UK*

<sup>3</sup>*Steward Observatory, University of Arizona, 933 North Cherry Avenue, Tucson, AZ 85721, USA*

<sup>4</sup>*Astrophysics Science Division, X-ray Astrophysics Laboratory, Code 662, NASA Goddard Space Flight Center, Greenbelt, MD 20771, USA*

<sup>5</sup>*INAF – Osservatorio Astronomico di Brera, via E. Bianchi 46, I-23807 Merate, Italy*

<sup>6</sup>*Dipartimento di Fisica “G. Occhialini”, Università di Milano – Bicocca, Piazza della Scienza 3, I-20126 Milano, Italy*

<sup>7</sup>*Center for Astrophysics, Guangzhou University, Guangzhou 510006, China*

<sup>8</sup>*Department of Astronomy, School of Physics, Peking University, Beijing 100871, China*

<sup>9</sup>*Kavli Institute for Astronomy and Astrophysics, Peking University, Beijing 100871, China*

Accepted XXX. Received YYY; in original form ZZZ

## ABSTRACT

A brief *Chandra* observation of the ultraluminous quasar, SDSS J010013.02+280225.8 at redshift 6.326, showed it to be a relatively bright, soft X-ray source with a count rate of about 1 ct/ks. In this paper we present results for the quasar from a 65 ks *XMM-Newton* observation, which well constrains its spectral shape. The quasar is clearly detected with a total of  $\sim 460$  net counts in the 0.2–10 keV band. The spectrum is characterised by a simple power-law model with photon index of  $\Gamma = 2.30^{+0.10}_{-0.10}$ , and the intrinsic 2–10 keV luminosity is  $3.14 \times 10^{45}$  erg s<sup>-1</sup>. The  $1 \sigma$  upper limit to any intrinsic absorption column density is  $N_H = 6.07 \times 10^{22}$  cm<sup>-2</sup>. No significant iron emission lines were detected. We derive the X-ray-to-optical flux ratio  $\alpha_{\text{ox}}$  of  $-1.74 \pm 0.01$ , consistent with the values found in other quasars of comparable ultraviolet luminosity. We did not detect significant flux variations either in the *XMM-Newton* exposure or between *XMM-Newton* and *Chandra* observations, which are separated by  $\sim 8$  months. The X-ray observation enables the bolometric luminosity to be calculated after modelling the spectral energy distribution: the accretion rate is found to be sub-Eddington.

**Key words:** quasar: individual: SDSS J010013.02+280225.8 – galaxies: active – galaxies: high-redshift

## 1 INTRODUCTION

SDSS J010013.02+280225.8 (hereafter J0100+2802) is an ultraluminous quasar at redshift of 6.326, which has an optical and infrared luminosity several times greater than any other high redshift quasars and is inferred to host a  $10^{10} M_{\odot}$  black hole (Wu et al. 2015). The quasar is clearly detected in the exploratory *Chandra* observation with exposure of 14.8 ks, found to have a steep spectrum with  $\Gamma = 3.03^{+0.78}_{-0.70}$  derived from the detected 14 counts (Ai et al. 2016). This super-massive black hole might be growing with rapid accretion, as the bolometric luminosity yielded from X-ray to near-infrared observations close to the Eddington luminosity (Wu et al. 2015; Ai et al. 2016). With the peculiar properties among all quasars discovered at  $z \gtrsim 5$ , which

are powerful probes of cosmic reionization (Fan et al. 2006), J0100+2802 sets the tightest constraints on models for massive black hole growth and evolution at early epochs (e.g. Shankar et al. 2009; Volonteri 2010).

In *Chandra* observation, the X-ray-to-optical flux ratio of J0100+2802 is at upper envelop of the observed  $\alpha_{\text{ox}}$  values at the comparable ultraviolet luminosity, reported in the Erratum to that paper (Ai et al. 2017). Quasars are of known to be variable and it is quite possible that this one has been caught in a bright state. The  $z=7.1$  quasar, ULASJ1120+0641, is claimed to decrease in brightness by a factor of 4 between *Chandra* and *XMM-Newton* observation (Page et al. 2014), although debate exists (Moretti et al. 2014). There are hints of variation of J0100+2802 during the *Chandra* exposure, which is quite puzzling if no significant beaming effect evolved. For high redshift quasars extended X-ray lobes may be produced via Comptonization of cosmic

★ E-mail: aiyanli@mail.sysu.edu.cn

microwave background (CMB) if relativistic electrons exist (Fabian et al. 2014).

We proposed for a *XMM-Newton* Director’s Discretionary Time (DDT) observation of J0100+2802 which would yield an improved spectrum with greatly reduced errors on the spectral index, and enable a search for any spectral features. Comparison of the flux with that from *Chandra* would provide a check on variability. Extended lobes produced from inverse Compton scattering of CMB, which may extend over arcmin scales, could be detected with *XMM-Newton*. In this letter we report the spectral properties of this ultraluminous quasar from the *XMM-Newton* observation. Throughout this paper, we adopt the  $\Lambda$ CDM cosmology parameters from Planck Collaboration (2014):  $\Omega_M = 0.315$ ,  $\Omega_\Lambda = 0.685$ , and  $H_0 = 67.3 \text{ km s}^{-1}$ . We define power law photon index  $\Gamma$  such that  $N(E) \propto E^{-\Gamma}$ . For the Galactic absorption of SDSS J0100+2802, which is included in the model fitting, we use the value of  $N_H = 5.82 \times 10^{20} \text{ cm}^{-2}$  (Kalberla et al. 2005). All uncertainties are given at  $1\sigma$ , unless otherwise specified.

## 2 XMM-NEWTON OBSERVATION AND DATA REDUCTION

J0100+2802 was observed with *XMM-Newton* on 2016 June 29 for 65 ks of Director’s Discretionary Time. The European Photon Imaging Camera (EPIC) was operated in full-frame mode, with thin filters. The data were processed using the Science Analysis System (SAS) version 15.0.0. The time intervals of high flaring backgrounds contamination were identified and excluded by inspection of the light curves in the 10-12 keV energy range. The total cleaned exposure times are 50 and 60 ks for the PN and MOS cameras, respectively. Event patterns 0-12 were included in the MOS cameras, while for the PN camera we used patterns 0-4. We constructed the images in five bands, 0.2-0.5 keV, 0.5-4 keV, 4-7 keV, 7-10 keV, and then applied source detection simultaneously using the standard SAS task EDETECT\_CHAIN.

We extract a spectrum of J0100+2802 from a  $16''$  radius region around the target in each EPIC detector. The source-extraction region corresponding to 60%-70% of the encircled energy fraction. The background was extracted from an adjacent source-free region with a larger radius. The spectra of the target from PN/MOS cameras were combined to form a single spectrum, with corresponding background spectra and response matrices also combined to form a single background spectrum and response matrix, with SAS task epic-speccombine. The EPIC spectra are then grouped in a way that there are at least 25 counts in each energy bin. We only focus on spectrum analysis in this paper.

## 3 RESULTS

As shown in Figure 1, J0100+2802 is clearly detected in the *XMM-Newton* EPIC images. The most accurate source position, from the VLBA 1.5 GHz image, lies within the astrometric uncertainties of both the optical Sloan Digital Sky Survey and the *Chandra* X-ray observation (Wang et al. 2017). The XMM X-ray position of the quasar given by SAS

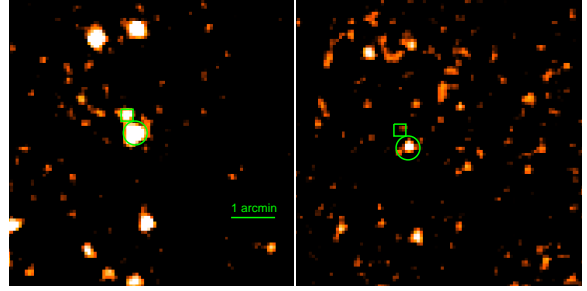


**Figure 1.** The  $2''$  kernel smoothed *XMM-Newton* PN image of J0100+2802 region of the sky in the observed 0.3-2 keV (left panel) and 2-10 keV (right panel). The circle indicates the radius used to extract the spectrum, and the square indicates the location of the nearby X-ray source SDSS J010013.95+280250.6.

task EDETECT\_CHAIN is  $\sim 1.7$  arcsec away from the radio position, with a  $1\sigma$  position uncertainty of 0.6 arcsec.

The detected net counts of J0100+2802 in 0.2-10 keV is 460. J0100+2802 is relatively soft with weak detection in hard X-ray band, 2-10 keV (Figure 1). It is detected individually in 0.2-0.5 keV and 0.5-4 keV with false probability less than  $10^{-10}$ ; While, in 4-7 keV the detection significance of the quasar is close to 3 sigma with a false probability of 0.015. It is not detected in the 7-10 keV band.

The nearby X-ray source, SDSS J010013.95+280250.6, which is detected in *Chandra* observation  $28''$  to the north-east of J0100+2802, is also detected in the *XMM-Newton* EPIC image (Figure 1). This object is relatively faint in X-ray emission with detected net counts of 80 in 0.2-10 keV within a  $15''$  radius aperture in the EPIC images. It is not detected in the hard X-ray band (2-10 keV in the observed frame) with an upper limit of  $10^{-4} \text{ cnt s}^{-1}$  estimated from the sensitivity maps using the SAS task *esensmap* for a logarithmic likelihood of 12. According to the Point Spread Function, the counts from this faint object, which fall in the source extraction region of our target quasar, are  $\sim 8$  counts. Our target quasar therefore has little contamination from its emission.

The image of J0100+2802 appears slightly lop-sided to the South East, as shown in Figure 2. The excess flux in 0.5-2 keV is about  $2 \times 10^{-16} \text{ erg s}^{-1} \text{ cm}^{-2}$ . A deep *Chandra* image is required to distinguish several unresolved faint point sources from possible diffuse inverse Compton emission. If it is the latter due to a jet from the quasar then it may be detectable in the radio band below the mJy level.

We fitted the spectrum of J0100+2802 using XSPEC (v12.9; Arnaud 1996) using a simple power-law model modified by Galactic absorption. The fitted photon index is  $\Gamma = 2.30^{+0.10}_{-0.10}$ . The fit is acceptable, with a  $\chi^2 = 24.7$  for 23 degrees of freedom (Figure 3). We also fold the model with intrinsic absorption (at  $z=6.326$ ). There is no significant improvement with  $\Delta\chi^2$  of 1.7, and  $1\sigma$  upper limit of the intrinsic absorption column density is  $N_H = 6.07 \times 10^{22} \text{ cm}^{-2}$ . There are residuals at energy between 5-10 keV, as shown in Figure 3, which are possibly due to contamination from background as the source detection significance in this energy range is below 3 sigma. The rest-frame 2-10 keV luminosity implied by the fit is  $3.14^{+0.53}_{-0.48} \times 10^{45} \text{ erg s}^{-1}$ .

No Fe K emission line feature appears to be present in the residuals, and the  $1\sigma$  upper limit for the iron  $K\alpha$  equiv-

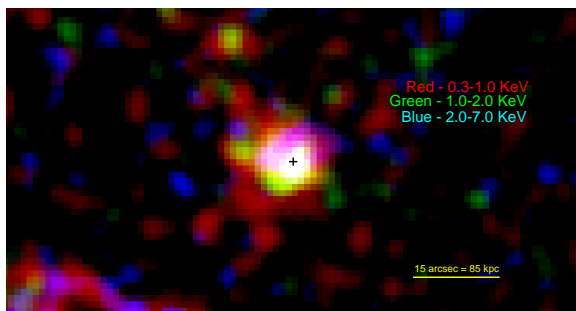


**Figure 2.** A RGB color image of J0100+2802 using different bands from the EPIC PN image. Red shows soft X-ray emission (0.3-1.0 keV), green shows intermediate emission (1.0-2.0 keV) and blue shows the hard X-ray emission.

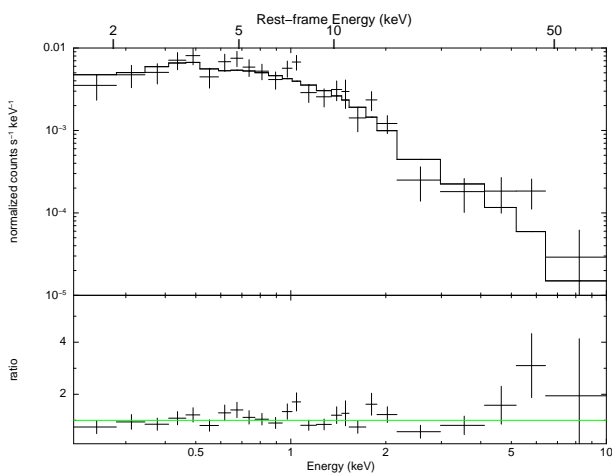


**Figure 3.** Upper panel: *XMM-Newton* spectrum of J0100+2802 and power-law model with fixed Galactic absorption. Lower panel: ratio of the data to model. The relatively larger data to model ratio at energies greater than 4 keV maybe due to dominance of X-ray background emission above 4 keV for this quasar.

alent width is 0.02 keV (rest frame). There are relatively larger data to model ratio at energies greater than 5 keV (rest frame  $\sim 36$  keV), which are possibly due to the contamination from statistical poisson fluctuation of the background emission. As shown above, the detected significance of J0100+2802 at 4-7 keV is only at the level of  $3\sigma$ . Further deep exposures can help to justify whether the spectral shape of this quasar deviates from a simple power-law at high energies.

The light curve for J0100+2802 is extracted and no significant variation is detected during the *XMM-Newton* exposure. We then compare the X-ray spectrum and flux between the *Chandra* and *XMM-Newton* observations with time interval of about 8 months. First, the value of the inferred photon index from *XMM-Newton* observation is within the errors of the one from *Chandra* observation, which is  $\Gamma = 3.03^{+0.78}_{-0.70}$ . That is, no statistical spectral shape variation was detected between the two observations for J0100+2802. Second, there is none detection of flux variation between the two observations, with the rest-frame 2-10 keV luminosity implied by the fit in *XMM-Newton* observation consistent within errors with the one,  $9.0^{+9.1}_{-4.5} \times 10^{45}$  erg  $s^{-1}$ , from *Chan-*

*dra* observation. Finally, the residual at  $\sim 1.2$  keV, hinted at in the *Chandra* spectrum of J0100+2802, was not detected. The non-detection in *XMM-Newton* observation indicates that the feature in *Chandra* spectrum was probably due to instrumental lines (Bartalucci et al. 2014), although Poisson fluctuation can not be excluded.

## 4 DISCUSSION

J0100+2802 is significantly detected in the *XMM-Newton* observation with total net counts of 460 in the 0.2-10 keV band. A simple power-law model provides acceptable fits to the spectrum with inferred photon index of  $\Gamma = 2.30^{+0.10}_{-0.10}$ . The value of  $\Gamma$  is consistent with the one found by Nanni et al. (2017). The  $1\sigma$  upper limit on any intrinsic absorption column density is  $N_H = 6.07 \times 10^{22} \text{cm}^{-2}$ . No significant iron emission lines were detected. With the well constrained X-ray spectral shape and luminosity, we now discuss the emission from accretion disk with broad-band energy spectral analysis for J0100+2802, and compare the spectral energy distributions (SED) of this quasar with other high-redshift and low-redshift quasars.

### 4.1 Black hole mass and disc luminosity of J0100+2802

The black hole mass estimated by Wu et al. (2015) is  $M_{\text{BH}} = 1.2 \times 10^{10} M_{\odot}$ . This is based on the virial method, and it is therefore affected by an uncertainty of a factor 3 (acknowledged by Wu et al. 2015). The bolometric luminosity, assumed isotropic, given by Wu et al. (2015), is  $L_{\text{bol}} = 1.6 \times 10^{48}$  erg  $s^{-1}$ , and includes the infrared and the X-ray emission (following Shen et al. 2011). The corresponding optical-UV emission is nearly 1/2 of that (Calderone et al. 2013). The other half is reprocessed emission in the infrared by the absorbing torus surrounding the disc, plus the X-ray emission produced by the corona sandwiching the disc. The latter could indeed be energised by the gravitational energy of the accreting matter.

Both the black hole mass and the accretion luminosity are huge, and motivate us to explore alternative methods to reliably measure them. A proper accretion luminosity estimate should exclude the infrared reprocessed emission and take into account possible anisotropies. We therefore use a standard Shakura & Sunyaev (1973) accretion disc model to fit the observed optical-UV flux, while the corona X-ray emission is treated phenomenologically by adding a power law starting below the peak of the disk emission, ending with an exponential cut. This component requires three parameters: normalization, slope and cut frequency.

We are aware of the limitations connected with the use of the Shakura-Sunyaev disk model, mainly due to i) the spin is assumed to be zero; ii) all relativistic effects are neglected and iii) the disk is assumed to be geometrically thin and optically thick. The first assumption would lead to a *lower limit* on the black hole mass and to an *upper limit* on the accretion rate, as discussed below. The second assumption introduces an uncertainty on the angular pattern of the produced radiation, but not on the overall shape of the spectrum (see, e.g. Campitiello et al. 2017). The latter assumption is questionable in the case of near (or above)

Eddington accretion, since because the disk could become geometrically thicker close to the black hole.

Assuming a null spin implies an innermost radius of the circular orbit ( $R_{\text{ISCO}} = 6R_g$ ,  $R_g$  is the gravitational radius) and a corresponding accretion efficiency (defined by  $L = \eta \dot{M} c^2$ ) equal to 0.057 or to 0.08 according if relativistic effects are included or not. By increasing the spin,  $R_{\text{ISCO}}$  decreases, to become  $R_g$  when the dimensionless spin  $a \sim 1$ . Correspondingly,  $\eta$  increases, reaching a theoretical maximum of 0.42, that is however reduced to  $\eta = 0.32$  (Thorne 1974) when properly including the effects of accretion (and of photons produced by the disk falling into the black hole). The black hole spin has a negligible effect on the outer regions of the disk emitting in the infrared–optical band, but changes the emitting properties of the inner radii. In other words, for a given accretion rate and black mass, the disk around a rotating hole will produce the same amount of IR radiation, but more UV than a Shakura–Sunjaev disk.

The SED of J0100+2802 shows indeed a peak, allowing to find the total luminosity, associated to the accretion rate for the assumed efficiency  $\eta$ , and the black hole mass, since the peak frequency is associated to the temperature of the innermost orbits contributing to the observed spectrum. Applying the Shakura–Sunjaev model (i.e. zero spin) we then find  $M$  and  $\dot{M}$ . If we assume a non-zero and positive spin, the total luminosity can be produced with a reduced accretion rate ( $\eta$  is larger), but this implies that we underestimate the flux in the optical–IR bands (flux produced at larger radii). Therefore we have to increase the black hole mass (and therefore the surface of the disk) to make the disk “colder” in order to fit the entire spectrum.

We consider the anisotropic emission of the disc, that follows a pattern  $\propto \cos \theta$ , and assume that object is observed under a viewing angle  $30^\circ$  from the disc’s normal (i.e. the average angle between  $0^\circ$  and an assumed aperture angle of the torus of  $45^\circ$ ). Along with the disc emission, we assume a blackbody emission at a temperature  $T_{\text{torus}}$  to model the torus emission. For the corona X–ray component, as explained above, we assume a power law of photon index  $\Gamma = 2.5$  ending with an exponential cut ( $h\nu_{\text{cut}} = 300$  keV), emitting a fraction  $L_x/L_{\text{disc}} \sim 1/3$  of the optical–UV luminosity. The infrared and X–ray fluxes are assumed to be emitted isotropically.

Figure 4 shows the infrared to X–ray spectral energy distributions (SED) of J0100+2802, together with the fitting model. The disc optical–UV luminosity is  $L_{\text{disc}} \sim 3.7 \times 10^{47}$  erg s $^{-1}$ , that corresponds to 32% of the Eddington luminosity, for a black hole mass of  $M_{\text{BH}} = 9 \times 10^9 M_\odot$ , slightly smaller than the estimate of Wu et al. (2015), but still consistent. The total X–ray luminosity (i.e. from the peak frequency of the disc emission to  $\sim 1$  MeV) is  $\sim 1/3$  of  $L_{\text{disc}}$ . This gives  $L_x + L_{\text{disc}} \sim 5 \times 10^{47}$  erg s $^{-1}$ , equivalent to  $0.43 L_{\text{Edd}}$ . As explained above, the assumption of zero spin, implicit in the use of the Sakura–Sunjaev model, implies that the derived value of the black mass is a lower limit. This strongly suggests that the disk luminosity, including the rather large X–ray component, is sub–Eddington. The uncertainty of the derived black hole mass is  $\sim 0.4$  dex, as shown in Figure 5. In the figure we show the SED modelling of J0100+2802, corresponding to the same luminosity, but with different masses.

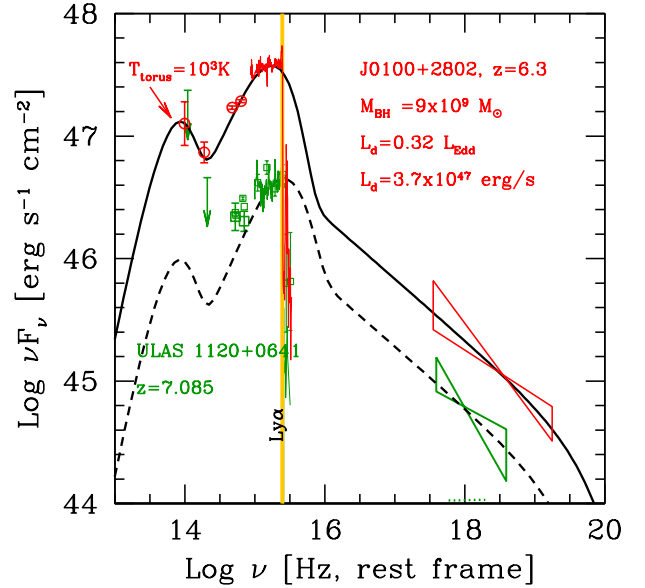


**Figure 4.** The spectral energy distributions of J0100+2802 (symbols in red) and our fitting model (solid black line) compared to the SED (symbols in green) and model (dashed black line) of ULAS J1120+0641. The vertical orange line labels the Ly $\alpha$  line. The inferred black hole mass and accretion luminosity for J0100+2802 are indicated. Infrared data are from WISE, optical spectra from the works by Mortlock et al. (2011) and Wu et al. (2015), respectively. X–rays of J0100+2802 are from this work.

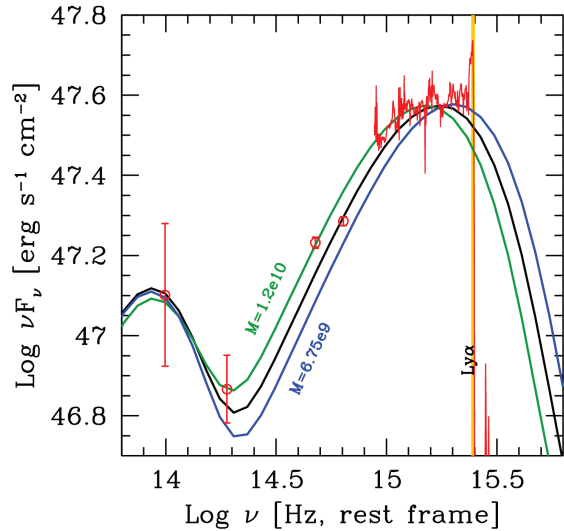


**Figure 5.** SED modelling of J0100+2802, corresponding to the same total luminosity, but with three different masses (solid black line is the one with mass of  $9 \times 10^9 M_\odot$ ).

## 4.2 Comparison with ULAS J1120+0641

Figure 4 includes the SED of ULAS 1120+0641, the quasar with the largest measured redshift ( $z = 7.085$ ; Mortlock et al. 2011). In the far-infrared band we have only upper limits to the flux, that are not very constraining. Note also some discrepancy between the photometric and the spectral data at the same frequencies. For the fit, we have given priority to the spectroscopic data.

This source is less luminous than J0100+2802, and its mass is smaller, according to the estimate obtained by fitting the SED. With the same accretion disc model as before, in fact, we obtain  $M_{\text{BH}} = 1.3 \times 10^9 M_{\odot}$ ;  $L_{\text{disc}} = 3.9 \times 10^{46} \text{ erg s}^{-1} = 0.23 L_{\text{Edd}}$ ;  $L_X = 0.8 L_{\text{disc}} \sim 3 \times 10^{46} \text{ erg s}^{-1}$  and  $L_X + L_{\text{disc}} = 0.41 L_{\text{Edd}}$ . As previously explained for J0100+2802, the value of the black hole mass should be taken as a lower limit. We conclude that both sources, despite the difference of black hole mass, share similar Eddington ratios and similar partition between optical-UV and X-ray luminosities. We can compare our results on ULAS J1120+0641 with the ones of Mortlock et al. (2011) who found  $M_{\text{BH}} \sim 2 \times 10^9 M_{\odot}$  (through the virial method) and a disc luminosity of  $2.5 \times 10^{47} \text{ erg s}^{-1}$  (applying a fiducial bolometric correction taken from Willott et al. (2010)). Differently from us, the results of Mortlock et al. (2011) indicate a slightly super-Eddington luminosity.

## 4.3 Comparison with other powerful quasars

It is well established that the X-ray-to-optical power-law slope parameter  $\alpha_{\text{ox}}$  of quasars significantly correlate with the ultraviolet 2500Å monochromatic luminosity ( $L_{2500\text{\AA}}$ , Steffen et al. 2006; Just et al. 2007). For J0100+2802 with rest frame 2500Å flux density,  $f_{2500\text{\AA}}$ , estimated from Wu et al. (2015) and rest-frame 2 keV flux density,  $f_{2\text{ keV}}$ , estimated from the power law model, we have the parameter  $\alpha_{\text{ox}}$  of  $-1.74 \pm 0.01$ . In Figure 6, we show the location of J0100+2802 and the other highest-redshift quasars with  $z > 6$ , of which we take the  $\alpha_{\text{ox}}$  and  $L_{2500\text{\AA}}$  from literatures (Brandt et al. 2002; Farrah et al. 2004; Shemmer et al. 2006; Moretti et al. 2014; Page et al. 2014; Gallerani et al. 2017), in the  $\alpha_{\text{ox}}-L_{2500\text{\AA}}$  relation. It is clear that the SED of the ultra-luminous J0100+2802 is not abnormal among the highest redshift quasars and all the quasars at  $z > 6$  follow the  $\alpha_{\text{ox}}-L_{2500\text{\AA}}$  relation as the low- and median-redshift quasars. As discussed in Nanni et al. (2017), which presents a systematic analysis of X-ray archival data of quasars at  $z > 5.5$ , these results support the non-evolutionary scenario of the SEDs of luminous quasars. For J0100+2802 the inferred value of  $\alpha_{\text{ox}}$  in Nanni et al. (2017) is  $-1.88^{+0.01}_{-0.02}$ , which is in agreement with ours considering the scatter of the  $\alpha_{\text{ox}}-L_{2500\text{\AA}}$  relation.

With rest-frame equivalent width of the Ly $\alpha$  + Nv  $\sim 10\text{\AA}$  (Wu et al. 2015), J0100+2802 is one of the Weak-line quasars (WLQs), which are a subclass of radio-quiet quasars that have almost extremely weak or undetectable emission lines (e.g. Fan et al. 1999; Meusinger & Balafkan 2014, and references therein). Significant fractions ( $\sim 50\%$ ) of the WLQs are distinctly X-ray weak compared to typical quasars (Shemmer et al. 2009; Wu et al. 2012; Luo et al. 2015). While, as shown in Figure 6, J0100+2802 is not X-ray weak, compared to the SEDs of the other WLQs.

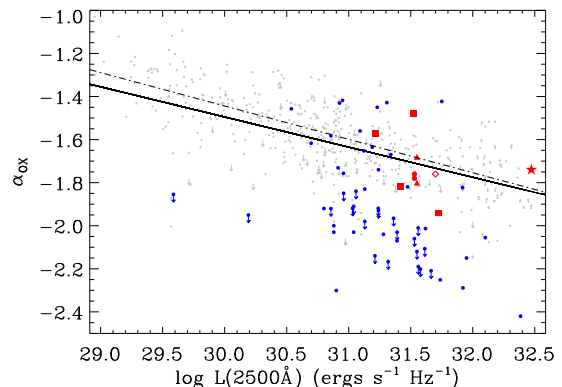


**Figure 6.** Location of J0100+2802 (red star) in the X-ray-to-optical power-law slope parameter  $\alpha_{\text{ox}}$  vs. 2500 Å monochromatic luminosity. The grey dots are the quasars from the samples of Just et al. (2007); Steffen et al. (2006) and Gibson et al. (2008). The blue dots are the weak line quasars and PHL 1811 analogs from Luo et al. (2015). The solid line represents the  $\alpha_{\text{ox}}-L_{2500\text{\AA}}$  relation from Just et al. (2007) and the dotted-dashed line from Nanni et al. (2017). The red symbols represent the high-redshift quasars with  $z > 6.0$  from literatures (squares from Shemmer et al. (2006), filled circles of ULAS J1120+0641 (Moretti et al. 2014; Page et al. 2014), triangles of SDSSJ1030 (Brandt et al. 2002; Farrah et al. 2004), and diamonds of SDSSJ1148+5152 (Gallerani et al. 2017)).

J0100+2802, presented as an X-ray normal weak-line quasar, provides constraints about the proposed hypotheses to the interpretation of weak-line quasars, such as a soft ionizing spectral energy distribution due to intrinsic X-ray weakness or due to small-scale absorption (e.g., Leighly et al. 2007; Wu et al. 2012; Luo et al. 2015).

We did not detect variation of the X-ray emission for J0100+2802 in the XMM-Newton exposure, and no significant variation was detected in the X-ray flux observed from XMM-Newton and Chandra observations. For this high-redshift radio-quiet luminous quasar, the non-detection of variation is not un-expected. Also, the results normally rule out the possibility from jet beaming effect in the observed X-ray brightness of J0100+2802, in which case there should be detected variations.

## 5 SUMMARY

With the well-detected X-ray emission from XMM-Newton observation, J0100+2802 presents as an peculiar high-redshift quasar in X-ray with relatively soft X-ray spectral shape. With the X-ray observation, the bolometric luminosity is calculated from spectral energy distributions modelling and the accretion rate is estimated to be sub-Eddington. The location in the  $\alpha_{\text{ox}}-L_{2500\text{\AA}}$  relation indicates it is an X-ray normal quasar either in term of high-redshift quasars or weak-line quasars. The results from XMM-Newton observation of J0100+2802 are meaningful for the study of quasar X-ray properties, broad-band energy distribution, and super-massive black hole formation and evolution at cosmic dawn.

**ACKNOWLEDGEMENTS**

Y.-L.A. and L.L.F. acknowledge the support from the NSFC grants 11273060, 91230115 and 11333008, and State Key Development Program for Basic Research of China (No. 2013CB834900 and 2015CB857000). A.C.F. and S.A. W. acknowledge support from ERC Advanced Grant 340442. S.A.W. was also supported by an appointment to the NASA Postdoctoral Program at the Goddard Space Flight Center, administered by USRA through a contract with NASA. X.F. acknowledges support from NSF grant AST 15-15115 and from the Institute of Astronomy, University of Cambridge through a Raymond and Beverly Sackler Distinguished Visitor program. F.W. and X.-B.W. acknowledge the support from NSFC grants 11373008 and 11533001. We thank Tinggui Wang, and Junxian Wang for helpful discussions. This work is based in part on observations obtained with *XMM-Newton*, an ESA science mission with instruments and contributions directly funded by ESA Member States and NASA. We thank Dr Norbert Scharrel for the allocation of XMM observing time.

**REFERENCES**

- Ai, Y.L., Dou, L.M., Fan, X., Wang, F.G., Wu, X.-B. & Bian, F.Y. 2016, *ApJL*, 823, 37
- Ai, Y.L., Dou, L.M., Fan, X., Wang, F.G., Wu, X.-B. & Bian, F.Y. 2017, *ApJL*, submitted
- Arnaud, K. A. 1996, in *Astronomical Society of the Pacific Conference Series*, Vol. 101, *Astronomical Data Analysis Software and Systems V*, ed. G. H. Jacoby & J. Barnes, 17
- Bartalucci, I., Mazzotta, P., Bourdin, H. & Vikhlinin, A. 2014, *A&A*, 566, 25
- Brandt, W.N., Schneider, D.P., Fan, X.H., et al. 2002, *ApJ*, 569, 5
- Calderone, G., Ghisellini, G., Colpi, M., Dotti, M., 2013, *MNRAS*, 431, 210
- Campitiello, S., Ghisellini, G., Sbarrato, T. & Calderone, G., arXiv1702.00011
- Fabian, A. C., Walker, S. A., Celotti, A., et al. 2014, *MNRAS*, 442, 81
- Fan, X., Strauss, M. A., Gunn, J. E., et al. 1999, *ApJ*, 526, L57
- Fan, X., Carilli, C. L. & Keating, B. 2006, *ARA&A*, 44, 415
- Farrah, D., Priddey, R., Wilman, R., Haehnelt, M. & McMahon, R. 2004, *ApJ*, 611, 13
- Gallerani, S., Zappacosta, L., Orofino, M. C., et al. 2017, *MNRAS*, 467, 3590
- Gibson, R. R., Brandt, W. N., & Schneider, D. P. 2008, *ApJ*, 685, 773
- Just, D.W., Brandt, W.N., Shemmer, O., et al. 2007, *ApJ*, 665, 1004
- Kalberla, P. M. W., Burton, W. B., Hartmann, D., et al. 2005, *A&A*, 440, 775
- Leighly, K. M., Halpern, J. P., Jenkins, E. B., & Casebeer, D. 2007, *ApJS*, 173, 1
- Luo, B., Brandt, W. N., Hall, P. B., et al. 2015, *ApJ*, 805, 122
- Meusinger, H., & Balafkan, N. 2014, *A&A*, 568, A114
- Moretti, A., Ballo, L., Braito, V., et al. 2014, *A&A*, 563, 46
- Mortlock, D.J, Warren, S. J., Venemans, B. P. et al., 2011, *Nature*, 474, 616
- Nanni, R., Vignali, C., Gilli, R., Moretti, A., & Brandt, W.N., arXiv:1704.08693
- Page, M. J., Simpson, C., Mortlock, D. J., et al. 2014, *MNRAS*, 440, 91
- Planck Collaboration, 2014, *A&A*, 571, 16
- Shemmer, O., Brandt, W. N., Schneider, D. P., et al. 2006, *ApJ*, 644, 86
- Shemmer, O., Brandt, W. N., Anderson, S. F., et al. 2009, *ApJ*, 696, 580
- Shakura N.I. & Sunyaev R.A., 1973, *A&A*, 24, 337
- Shankar, F., Weinberg, D. H., & Miralda-Escudé, J. 2009, *ApJ*, 690, 20
- Shen, Y., Richards, G. T., Strauss, M. A., et al., 2011, *ApJS*, 194, 45
- Steffen, A.T., Strateva, I., Brandt, W.N., et al. 2006, *AJ*, 131, 2826
- Thorne, K.S., 1974, *ApJ*, 191, 507
- Volonteri, M. 2010, *A&ARv*, 18, 279
- Wang, R., Momjian, E., Carilli, C. L., et al. 2017, *ApJ*, 835, 20
- Willott, C. J., Albert, L., Arzoumanian, D., et al. 2010, *AJ*, 140, 546
- Wu, J., Brandt, W. N., Anderson, S. F., et al. 2012, *ApJ*, 747, 10
- Wu, X.-B., Wang, F., Fan, X., et al. 2015, *Nature*, 518, 512

This paper has been typeset from a  $\text{\TeX}/\text{\LaTeX}$  file prepared by the author.